Biochemical and Biophysical Research Communications 433 (2013) 249–254

Contents lists available at SciVerse ScienceDirect

Biochemical and Biophysical Research Communications

journal homepage: www.elsevier.com/locate/ybbrc

Amino-acid substitutions at the domain interface affect substrate and allosteric inhibitor binding in α-isopropylmalate synthase from *Mycobacterium tuberculosis*

Frances H.A. Huisman [a], Christopher J. Squire [b,*], Emily J. Parker [a,*]

[a] Biomolecular Interaction Centre and Department of Chemistry, University of Canterbury, Christchurch, New Zealand
[b] Maurice Wilkins Centre for Molecular Biodiscovery, School of Biological Sciences, University of Auckland, Auckland, New Zealand

ARTICLE INFO

Article history:
Received 25 February 2013
Available online 13 March 2013

Keywords:
Leucine biosynthesis
Mycobacterium tuberculosis
Protein asymmetry
Multi-domain
Allosteric regulation
Domain interface

ABSTRACT

α-Isopropylmalate synthase (α-IPMS) is a multi-domain protein catalysing the condensation of α-ketoisovalerate (α-KIV) and acetyl coenzyme A (AcCoA) to form α-isopropylmalate. This reaction is the first committed step in the leucine biosynthetic pathway in bacteria and plants, and α-IPMS is allosterically regulated by this amino acid. Existing crystal structures of α-IPMS from *Mycobacterium tuberculosis* (*Mtu*IPMS) indicate that this enzyme has a strikingly different domain arrangement in each monomer of the homodimeric protein. This asymmetry results in two distinct interfaces between the N-terminal catalytic domains and the C-terminal regulatory domains in the dimer. In this study, residues Arg97 and Asp444 across one of these unequal domain interfaces were substituted to evaluate the importance of protein asymmetry and salt bridge formation between this pair of residues. Analysis of solution-phase structures of wild-type and variant *Mtu*IPMS indicates that substitutions of these residues have little effect on overall protein conformation, a result also observed for addition of the feedback inhibitor leucine to the wild-type enzyme. All variants had increased catalytic efficiency relative to wild-type *Mtu*IPMS, and those with an Asp444 substitution displayed increased affinity for the substrate AcCoA. All variants also showed reduced sensitivity to leucine and altered biphasic reaction kinetics when compared with those of the wild-type enzyme. It is proposed that substituting residues at the asymmetric domain interface increases flexibility in the protein, particularly affecting the AcCoA binding site and the response to leucine, without penalty on catalysis.

1. Introduction

Interactions of residues at enzyme domain interfaces can be critical for enzyme function, even if the domain interface in question is distant from the enzyme active site [1]. The enzyme α-isopropylmalate synthase (α-IPMS, EC 2.3.3.13) is of interest in the study of domain interfaces, as it is a multi-domain protein with an asymmetric oligomeric structure [2]. α-IPMS catalyses the condensation of α-ketoisovalerate (α-KIV) and acetyl coenzyme A (AcCoA) to form α-isopropylmalate – the first committed step in leucine biosynthesis in bacteria and plants. α-IPMS is activated by divalent metal ions (with a preference for Mg^{2+}) [3], and allosterically regulated by leucine in a non-competitive manner [4,5].

Most known α-IPMS orthologues are homodimeric [2,6], although some have been predicted to adopt a tetrameric form [7,8]. The only current full-length crystal structure of this protein shows an intricately associated, domain-swapped, asymmetric homodimer (Fig. 1 [2]). This structure, of α-IPMS from *Mycobacterium tuberculosis* (*Mtu*IPMS), reveals that each monomer in the protein is composed of two main domains: a $(\beta/\alpha)_8$-barrel catalytic domain and an allosteric regulatory domain with a $(\beta\beta\beta\alpha)_2$ fold. Separating these domains are two subdomains, one adjacent to the active site and composed of an α-helix and two small β-strands (subdomain I), the other adjacent to the regulatory domain and composed of three α-helices (subdomain II). In the dimer, the monomers are wrapped around each other such that subdomain I of one monomer sits over the active site of the other. It is in the cleft between subdomain I and the catalytic domain that the substrate AcCoA is predicted to bind adjacent to the other substrate α-KIV at the C-terminal end of the $(\beta/\alpha)_8$-barrel. Substitutions of two subdomain I residues (His379 and Tyr410) that protrude into the active site have been shown to affect leucine-mediated inhibition [9].

Leucine binds in *Mtu*IPMS at the interface of the two regulatory domains of the dimer (PDB code 3FIG) [2], and at a location about 50 Å from the enzyme active sites. No conformational change is

Abbreviations: α-IPMS, α-isopropyl malate synthase; α-KIV, α-ketoisovalerate; AcCoA, acetyl coenzyme A; *Mtu*IPMS, α-IPMS from Mycobacterium tuberculosis; SAXS, small angle X-ray scattering.

* Corresponding authors. Addresses: Department of Chemistry, University of Canterbury, Private Bag 4800, Christchurch 8140, New Zealand (E.J. Parker). School of Biological Sciences, University of Auckland, PO Box 92019, Auckland, New Zealand (C.J. Squire). Fax: +64 3 364 2110 (E.J. Parker).

E-mail addresses: c.squire@auckland.ac.nz (C.J. Squire), emily.parker@canterbury.ac.nz (E.J. Parker).

0006-291X/$ - see front matter © 2013 Elsevier B.V. All rights reserved.
http://dx.doi.org/10.1016/j.bbrc.2013.02.092

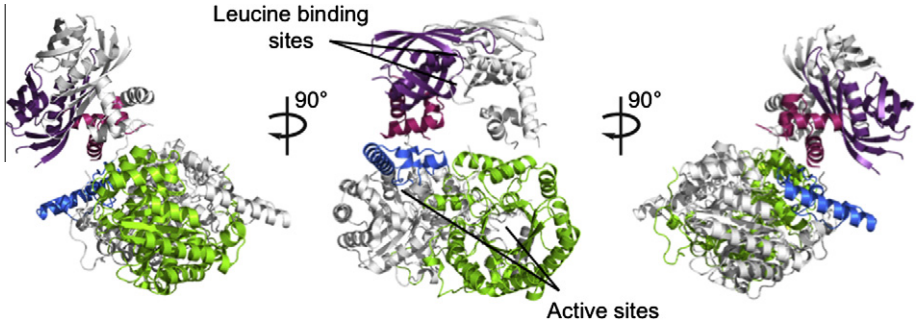

Fig. 1. *Mtu*IPMS crystal structure (PDB code 1SR9) [2]. One monomer shown in white, the other coloured by domain (catalytic domain in green, subdomain I in blue, subdomain II in pink and the regulatory domain in purple). Asymmetry is notable in the relative orientations of the regulatory domain and subdomain II compared to the catalytic domain and subdomain I. (For interpretation of the references to colour in this figure legend, the reader is referred to the web version of this article.)

apparent between the leucine bound and unbound *Mtu*IPMS structures that may account for the mechanism of inhibition [2], but hydrogen/deuterium exchange experiments suggest that the regulatory domain, subdomain II and an active site helix become more stable upon leucine binding [10]. It has been shown recently that the presence of the regulatory domain is critical for competent enzyme function for both *Mtu*IPMS and the α-IPMS from *Neisseria meningitidis* [11]. In contrast to other α-IPMS enzymes [5], *Mtu*IPMS undergoes slow-onset inhibition in the presence of leucine. This is caused by a transition from an initial Enz·Leu complex to a more tightly bound Enz*·Leu complex [4], a transition possibly mediated by the ordering of a flexible loop in the leucine binding site [12].

The asymmetry of *Mtu*IPMS is best described as a change in orientation of the C-terminal domains (the regulatory domain and subdomain II) relative to the N-terminal domains (catalytic domain and subdomain I). In monomer A, (coloured by domain in Fig. 1) the C-terminal domains form an interface with subdomain I, but in monomer B they interface with the monomer A catalytic $(\beta/\alpha)_8$-barrel. These two different interfaces can be thought of as the intra-monomeric domain interface and the inter-monomeric domain interface. Due to the asymmetry of the crystal structure, the interface residues in one monomer are spatially distant in the other.

It is unclear if the asymmetry apparent in the *Mtu*IPMS crystal structure plays any functional role in catalysis or as part of the allosteric communication system. It is also unknown if the asymmetrical state is the principal conformation of the protein in solution or if other conformations of the protein might be possible, for example whether transition from an asymmetric to a symmetric conformation takes place, or indeed a full interconversion between asymmetric conformational extremes. To investigate this, amino acid substitutions were made at the inter-monomeric domain interface, as this interface may play a key role in maintaining protein asymmetry. Variants were characterised to determine the importance of the inter-monomeric domain interface in *Mtu*IPMS structure and function.

2. Materials and methods

2.1. Mutagenesis to produce MtuIPMS-R97A, MtuIPMS-D444A, MtuIPMS-D444R and MtuIPMS-D444Y

Plasmids containing *Mtu*IPMS (pProExHTa-LeuA) were available from previous work [13]. Mutagenesis of plasmid pProExHTa-LeuA to achieve amino acid substitutions *Mtu*IPMS-R97A, *Mtu*IPMS-D444A, *Mtu*IPMS-D444R and *Mtu*IPMS-D444Y was carried out using 5′-phosphorylated plasmids and Phusion High-Fidelity DNA Polymerase (Finnzymes). The forward and reverse primers (Table S1, Supplementary Material) were designed to anneal back-to-back, rather than overlapping, allowing for greater success with multiple-base mismatches [14]. Reaction components and cycling parameters followed polymerase manufacturer's instructions. PCR amplification resulted in linear double-stranded DNA, which was purified using a 0.8% (w/v) E-Gel CloneWell Agarose Gel (Invitrogen) and re-circularised with T4 ligase overnight at room temperature. Sequencing was performed by Canterbury Sequencing on a ABI3100 Genetic Analyzer (Applied Systems Inc.) using a procedure based on Sanger chain-termination protocol. Sequence verified plasmids bearing the mutated *Mtu*IPMS genes were transformed into chemically competent *Escherichia coli* Rosetta 2 cell lines for expression.

2.2. Purification

Wild-type and variant *Mtu*IPMS proteins were purified by Talon affinity resin as described previously [11].

2.3. 4,4′-Dithiodipyridine-coupled assays at 324 nm

Initial velocity data were obtained using a 4,4′-dithiodipyridine-coupled assay at pH 7.5 and 25 °C as described previously [11]. Apparent K_m values were determined by varying one substrate while holding the other at a concentration of 250 μM and fitting rates to the Michaelis–Menten equation using Grafit [15], with typical errors less than 10% as determined from the fit to the equation.

2.4. SAXS data collection

Solution-phase structures of proteins were elucidated by SAXS on the Australian Synchrotron SAXS/WAXS beamline, with a 120 μm point source, camera length of 1.58 m, and exposure time of 2.0 s at 25 °C. Beam wavelengths were 1.127 Å for wild-type *Mtu*IPMS samples and 1.033 Å for variants *Mtu*IPMS-R97A, *Mtu*IPMS-D444A, *Mtu*IPMS-D444R and *Mtu*IPMS-D444Y. All samples were eluted from a Superdex 200 5/150 size-exclusion column (GE Healthcare) immediately prior to data collection.

Samples were analysed in 10 mM 1,3-bis[tris(hydroxymethyl)methylamino]propane buffer (pH 7.0), containing 100 mM KCl and 20 mM $MgCl_2$. For inhibition assays, protein was stored in buffer containing 1 mM L-leucine prior to data collection (in addition to buffer components above). Buffer used for the size-exclusion column during data analysis also contained 1 mM L-leucine.

2.5. SAXS data analysis

Primary data reduction was performed with ScatterBrain (www.synchrotron.org.au/index.php/aussyncbeamlines/saxswaxs/software-saxswaxs). Guinier fits were calculated by PRIMUS [16]

and AUTORG [17], and pair-distribution functions were calculated by GNOM [18]. Theoretical scattering plots were generated and fitted to experimental data by CRYSOL [19].

2.6. Molecular modelling of domain movement

Morph models for potential domain movement in *Mtu*IPMS crystal structure 1SR9 were generated using the RigiMOL package in PyMOL [20]. First the structure to be modelled was duplicated, and the duplicates aligned such that the $(\beta/\alpha)_8$-barrel of chain A in one copy of the structure was superimposed on the $(\beta/\alpha)_8$-barrel of chain B in the other, and *vice versa*. The alignment was performed with the *super* command over residues 1–368 in *Mtu*IPMS structure 1SR9, representing the catalytic domain of the protein. The overlaid duplicate structures were supplied as the beginning and end-points of the morph model. Morphing was performed with RigiMOL, using 10 refinement cycles and generating 20 transitional structures. The ninth and tenth structures of these were used for comparison to SAXS data as representing hypothetical symmetric *Mtu*IPMS enzymes.

3. Results

3.1. Amino acid substitution at the MtuIPMS inter-monomer interface

The inter-monomeric interface between the N- and C-terminal domains of *Mtu*IPMS occurs between the catalytic $(\beta/\alpha)_8$-barrel of one monomer and subdomain II of the other. This interface includes a salt bridge formed between residues Arg97 (catalytic domain) and Asp444 (subdomain II) that may act as an anchor for the C-terminal domains (Fig. 2). These residues are 31 Å from each other in the opposite barrel/subdomain pair.

In other α-IPMS orthologues, equivalents of Arg97 and Asp444 are found as long, polar residues with two potential hydrogen-bonding groups (arginine, glutamine, glutamate or aspartate). The bacterial α-IPMSs appear to favour Arg/Asp or Gln/Glu combinations, and this salt bridge may be a conserved feature of α-IPMS enzymes.

Variants *Mtu*IPMS-R97A and *Mtu*IPMS-D444A were designed to disrupt the inter-monomeric salt bridge, possibly making the protein less likely to adopt the conformation observed in the crystal structure. Further variants *Mtu*IPMS-D444R and *Mtu*IPMS-D444Y were created to change the polarity and steric bulk, respectively, of the aspartate location, in order to introduce some repulsion into this interface and possibly force a more symmetrical protein conformation. All four variants were successfully cloned, expressed and purified by metal-affinity chromatography. All variants formed dimers in solution, as determined by analytical gel filtration, with similar thermal stabilities to the wild-type protein (Table S3, Supplementary Material).

3.2. Solution-phase structure of MtuIPMS and variants

Solution-phase small angle X-ray scattering (SAXS) patterns were collected for wild-type protein in the presence and absence of leucine (Fig. 3) and for the four *Mtu*IPMS variants (Fig. S2, Supplementary Material). These data were compared to investigate potential conformational changes in protein solution-phase structure in variants *Mtu*IPMS-R97A, *Mtu*IPMS-D444A, *Mtu*IPMS-D444R and *Mtu*IPMS-D444Y, as well as any changes that may occur upon inhibitor binding. Details of structural parameters determining from the scattering data recorded for these proteins can be found in Table S4, Supplementary Material.

The scattering data for wild-type *Mtu*IPMS compare well with the theoretical scattering data curve generated from crystal structure 1SR9 [2], as shown in Fig. 3A. The slight differences between the experimental and theoretical scattering are likely due, at least in part, to the undefined residues and loops in the *Mtu*IPMS crystal structure. The comparison between theoretical and experimental scattering patterns indicates that *Mtu*IPMS is a dimer in solution, with a similar structure to that observed in crystal structure 1SR9.

To assess whether symmetry changes would be observable by SAXS, a model for a symmetrical homodimeric *Mtu*IPMS structure was generated. Comparison of the theoretical scattering from this model structure with the experimental data obtained for the enzyme reveals that the experimental data correspond more closely to those calculated for the asymmetric protein structure, than to the modelled symmetric structure. However, it should be noted that the difference between the theoretical scattering patterns for the observed crystal structure and modelled symmetrical structure is not large, and it is likely that the modelled symmetric structure only approximates that of any possible symmetric *Mtu*IPMS structure.

Data obtained in the presence and absence of leucine indicate that there is very little structural change upon leucine binding, in agreement with the observations made in the crystal structures (Fig. 3). Experimental data were compared to the calculated scattering patterns from crystal structures (PDB codes 3FIG and 1SR9, representing leucine-bound and unbound *Mtu*IPMS respectively). These crystal structures are nearly identical, and compare with an rms difference in Cα position of 0.23 Å for 965 residues. The calculated scattering profile from structure 1SR9 corresponds slightly more closely to the unliganded experimental data (Fig. 3A), whereas the scattering pattern calculated from structure 3FIG more closely resembles the data obtained in the presence of leucine (Fig. 3B). In both cases, the differences between theoretical scattering for structures 1SR9 and 3FIG were small, and it is

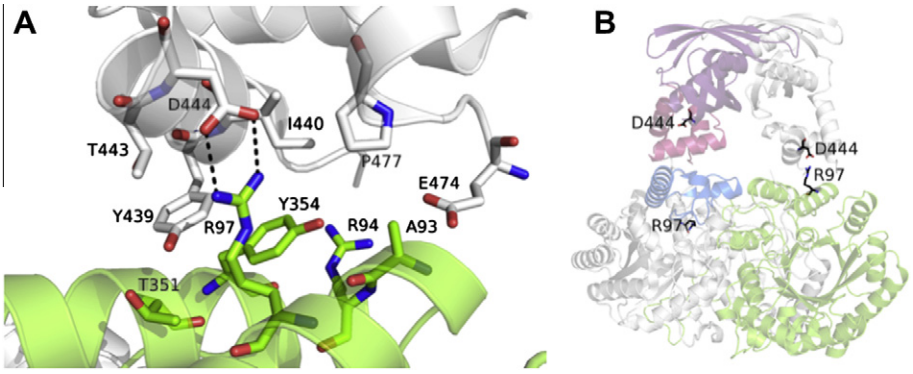

Fig. 2. Importance of residues Arg97 and Asp444 in *Mtu*IPMS. (A) Interface between the catalytic domain in one monomer and subdomain II of the other in *Mtu*IPMS structure 1SR9 [2]. Salt-bridge between Asp444 and Arg97 illustrated. (B) Positions of Arg97 and Asp444 in the asymmetric *Mtu*IPMS dimer.

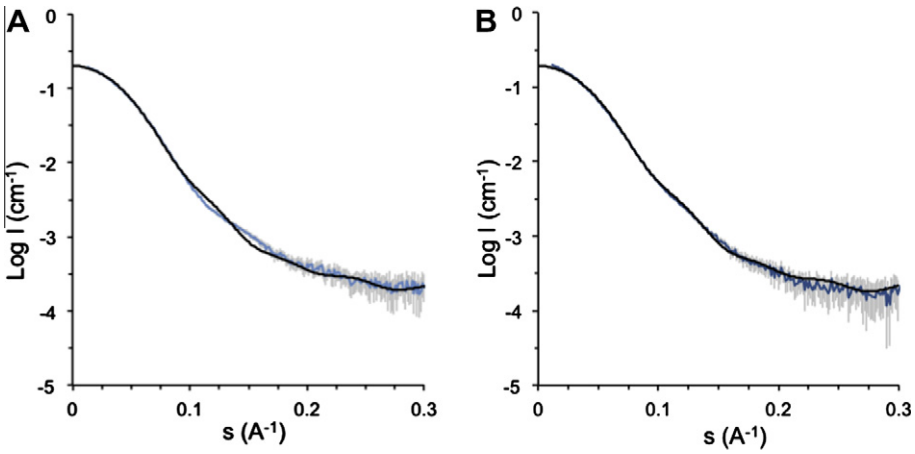

Fig. 3. Fits of theoretical scattering from *Mtu*IPMS crystal structures (black) to SAXS data from *Mtu*IPMS wild-type protein in the presence and absence leucine. (A) *Mtu*IPMS wild-type, theoretical scattering fitted from structure 1SR9, χ-value = 2.5; (B) *Mtu*IPMS wild-type with 1 mM leucine, theoretical scattering fitted from structure 3FIG, χ-value = 3.6.

Table 1
Kinetic data for wild-type and variant *Mtu*IPMS.

	K_m (μM)			k_{cat}/K_m (mM^{-1} s^{-1})	
Protein	α-KIV	AcCoA	k_{cat} (s^{-1})	α-KIV	AcCoA
Wild-type	15 ± 2	140 ± 20	3.7 ± 0.1	250 ± 40	27 ± 6
*Mtu*IPMS-R97A	8 ± 1	210 ± 20	7.0 ± 0.2	900 ± 100	33 ± 4
*Mtu*IPMS-D444A	5 ± 1	42 ± 5	3.1 ± 0.1	600 ± 100	70 ± 10
*Mtu*IPMS-D444R	9 ± 1	27 ± 3	5.7 ± 0.1	630 ± 80	210 ± 30
*Mtu*IPMS-D444Y	16 ± 1	42 ± 4	3.4 ± 0.1	210 ± 20	80 ± 10

apparent that *Mtu*IPMS does not show large changes to average structure in the presence of leucine, in line with previous observations from the crystal structures [2].

Scattering patterns for variants *Mtu*IPMS-R97A, *Mtu*IPMS-D444A, *Mtu*IPMS-D444R and *Mtu*IPMS-D444Y were compared to the experimental scattering of the wild-type protein (Fig. S2, Supplementary Material). These comparisons indicate that none of the substitutions are associated with significant changes in the protein structure.

It is apparent from these SAXS data that amino acid substitutions at the inter-monomeric domain interface of *Mtu*IPMS do not significantly affect overall structure, nor does the protein undergo major structural change in solution upon feedback inhibitor binding.

3.3. Kinetic characterisation of MtuIPMS and variants

All substitutions made at the inter-monomeric domain interface gave rise to catalytically active variants, which show similar affinities for α-KIV as the wild-type enzyme (Table 1) *Mtu*IPMS-D444A and *Mtu*IPMS-D444Y demonstrate similar turnover numbers to the wild-type enzyme, whereas *Mtu*IPMS-R97A and *Mtu*IPMS-D444R show a slight increase in this parameter. Compared to the wild-type protein, *Mtu*IPMS-R97A has slightly weaker affinity for AcCoA, whereas all three Asp444 substitutions demonstrate 3- to 5-fold stronger affinity for this substrate. All variants show some enhancement of catalytic efficiency over wild-type enzyme.

The *Mtu*IPMS variants were tested for their ability to be inhibited by the allosteric inhibitor leucine. *Mtu*IPMS-R97A, *Mtu*IPMS-D444A, *Mtu*IPMS-D444R and *Mtu*IPMS-D444Y all display the slow-onset inhibition [4] observed for wild-type *Mtu*IPMS (Fig. 4) but have weaker sensitivity to inhibition by leucine. This reduction in sensitivity appears to mostly affect the burst rate of the biphasic inhibition kinetics (Fig. 4A) suggesting that the formation of the initial Enz·Leu complex is affected more significantly by the substitutions than the transition to the Enz*·Leu complex. Both the *Mtu*IPMS variants with an Asp444 substitution display lower levels of inhibition for both burst and linear rates, whereas variant

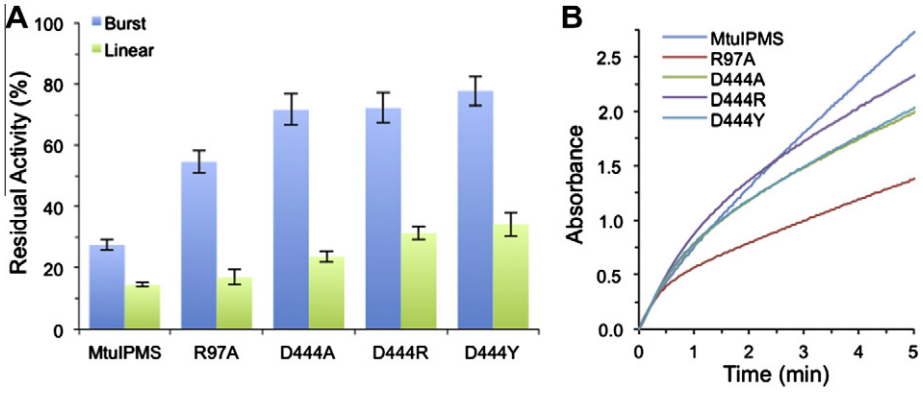

Fig. 4. Slow-onset inhibition in *Mtu*IPMS, *Mtu*IPMS-R97A, *Mtu*IPMS-D444A, *Mtu*IPMS-D444R and *Mtu*IPMS-D444Y in the presence of 1 mM L-leucine and 250 μM of each substrate. Buffer conditions are: 50 mM BTP (pH 7.5), 20 mM KCl and 20 mM $MgCl_2$. (A) Comparison of burst and linear rates for inhibition. Residual activity is calculated as a percentage of full activity (in the absence of L-leucine) for each variant. Burst rate is the initial rate in the presence of inhibitor and linear rate is the rate after slow-onset isomerisation of the Enz·Leu complex. (B) Differences in speed of slow-onset inhibition. Initial rates are scaled to 1 absorbance unit min^{-1}.

*Mtu*IPMS-R97A has a less inhibited burst rate, but similar linear rate, to wild-type enzyme.

Interestingly, the time required to undergo slow-onset inhibition was also altered by the domain-interface substitutions (Fig. 4B). In wild-type *Mtu*IPMS, this slow-onset transition occurs within the first minute of the reaction [4], but the Asp444 variants take almost twice as long to reach the linear phase of the reaction. These variants also show a much greater drop in activity from the Enz·Leu state to the Enz*·Leu state. If the slow-onset nature of inhibition is due to the flexible loop in the leucine binding site, in accordance with recent findings [12], then this change implies that the substitution of Asp444 affects the structure of the enzyme regulatory site, 20–30 Å away, or the communication pathway from this flexible regulatory loop to the active site.

4. Discussion

Amino acid substitutions *Mtu*IPMS-R97A, *Mtu*IPMS-D444A, *Mtu*IPMS-D444R and *Mtu*IPMS-D444Y affect both the catalytic and regulatory properties of *Mtu*IPMS, despite being located distant from both substrate and inhibitor binding sites. The substituted residues Arg97 and Asp444 are expected to be in close proximity in one half of the *Mtu*IPMS dimer, forming a salt bridge at the interface of the catalytic $(\beta/\alpha)_8$-barrel of one monomer and subdomain II of the other, but distant (~31 Å apart) in the other half of the structure. The inter-monomeric interface, and the salt bridge within it, may thus play a role in the asymmetry of the crystal structure and in the protein catalytic function and regulation.

α-KIV affinity and turnover number are similar in variants *Mtu*IPMS-R97A, *Mtu*IPMS-D444A, *Mtu*IPMS-D444R and *Mtu*IPMS-D444Y to values for wild-type protein, but AcCoA affinity is altered: decreasing slightly in *Mtu*IPMS-R97A and increasing 3- to 5-fold in the Asp444-substituted variants. The fact that each of the alanine substitutions across the salt bridge (*Mtu*IPMS-R97A and *Mtu*IPMS-D444A) display different kinetic parameters suggests that the residues have individual contributions to enzyme function in addition to this bond formation. All the variants demonstrate compromised sensitivity to leucine and the time taken to achieve full inhibition is decreased for the Asp444 variants. This change in slow-onset inhibition behaviour indicates that substitution of Asp444 affects the communication pathway between the leucine binding site and the active site or perhaps affects the properties of the leucine binding site itself.

While no obvious changes in structure of the protein are associated with the amino acid substitutions, it appears that substitutions to Arg97 and, especially, Asp444 do have some effect on both the regulatory domain and the AcCoA binding site. Other interactions at the catalytic-to-subdomain II interface appear to be mostly hydrophobic in nature. The only polar contacts evident in the structure, besides the salt bridge, are between the side chain of Arg94 and the main chain of Lys434, and the main-chain amino group of Ala93 and the side chain of Glu474. It is possible that these other interactions help to maintain the interface in the absence of the salt bridge, resulting in little overall change in asymmetric dimer structure. The loss of the Arg97-Asp444 contacts, however, may increase the flexibility of this region, in turn affecting the flexibility of adjacent domains and the ligand binding sites within them. This chain reaction of increased flexibility may account for the differences observed in substrate affinity and leucine sensitivity. Previous studies have shown similar unexpected propagation of changes for *Mtu*IPMS. Substitution of residue Tyr410 in subdomain I has been shown to alter flexibility in large regions of subdomain II [10], whereas substitution of active-site residue Glu218 decreases allosteric leucine affinity 10-fold [9]. One, perhaps surprising, effect of the Arg97 and Asp444 substitutions is the increased catalytic efficiency of the variant enzymes. It may be that increased protein flexibility aids catalytic activity, particularly the binding of AcCoA at the catalytic domain–subdomain I cleft. This would be in line with previous experiments correlating decreased flexibility of the enzyme with inhibition of catalytic activity by leucine [10].

An alternative explanation for the observed characteristics of the *Mtu*IPMS variants, as opposed to broadly increased enzyme flexibility, is that the amino acid substitutions act on a more local level to affect the binding of AcCoA. It could be that the increase in AcCoA affinity apparent in the Asp444 variants acts to diminish sensitivity to leucine. This decreased sensitivity mostly affects the initial burst rate of the inhibited enzyme (that is, the rate of the Enz·Leu complex), and transition to the Enz*·Leu conformation appears to reverse much of the inhibition-shielding provided. It is conceivable that the Asp444 substitutions act to increase flexibility in the AcCoA binding site, affecting the initial burst rate during inhibition, and rigidity is at least partially restored by the transition to the Enz*·Leu state, resulting in variant activity during the linear phase of inhibition that is almost the same as that seen in the wild-type. It appears that the competent molecular dynamics of *Mtu*IPMS are very sensitive to change, and that the rigidity of the inter-monomer domain interface is critical for the communication of allosteric inhibition in this enzyme.

Acknowledgments

This research was supported by funding from the Maurice Wilkins Centre for Molecular Biodiscovery and by the College of Science, University of Canterbury doctoral scholarship to FHAH. The SAXS data was collected at the SAXS/WAXS beamline at the Australian Synchrotron.

Appendix A. Supplementary data

Supplementary data associated with this article can be found, in the online version, at http://dx.doi.org/10.1016/j.bbrc.2013.02.092.

References

[1] T. Perica, J.A. Marsh, F.L. Sousa, E. Natan, L.J. Colwell, S.E. Ahnert, S.A. Teichmann, The emergence of protein complexes: quaternary structure, dynamics and allostery. Colworth Medal Lecture, Biochem. Soc. Trans. 40 (2012) 475–491.

[2] N. Koon, C.J. Squire, E.N. Baker, Crystal structure of LeuA from *Mycobacterium tuberculosis*, a key enzyme in leucine biosynthesis, Proc. Natl. Acad. Sci. USA 101 (2004) 8295–8300.

[3] L.P. de Carvalho, J.S. Blanchard, Kinetic analysis of the effects of monovalent cations and divalent metals on the activity of *Mycobacterium tuberculosis* α-isopropylmalate synthase, Arch. Biochem. Biophys. 451 (2006) 141–148.

[4] L.P. de Carvalho, A. Argyrou, J.S. Blanchard, Slow-onset feedback inhibition: inhibition of *Mycobacterium tuberculosis* α-isopropylmalate synthase by L-leucine, J. Am. Chem. Soc. 127 (2005) 10004–10005.

[5] F.H. Huisman, M.F. Hunter, S.R. Devenish, J.A. Gerrard, E.J. Parker, The C-terminal regulatory domain is required for catalysis by *Neisseria meningitidis* α-isopropylmalate synthase, Biochem. Biophys. Res. Commun. 393 (2010) 168–173.

[6] L.P. de Carvalho, J.S. Blanchard, Kinetic and chemical mechanism of α-isopropylmalate synthase from *Mycobacterium tuberculosis*, Biochemistry 45 (2006) 8988–8999.

[7] J.W. de Kraker, K. Luck, S. Textor, J.G. Tokuhisa, J. Gershenzon, Two *Arabidopsis* genes (IPMS1 and IPMS2) encode isopropylmalate synthase, the branchpoint step in the biosynthesis of leucine, Plant Physiol. 143 (2007) 970–986.

[8] T.R. Leary, G.B. Kohlhaw, α-Isopropylmalate synthase from *Salmonella typhimurium*. Analysis of the quaternary structure and its relation to function, J. Biol. Chem. 247 (1972) 1089–1095.

[9] L.P. de Carvalho, P. Frantom, A. Argyrou, J. Blanchard, Kinetic evidence for inter-domain communication in the allosteric regulation of α-isopropylmalate synthase from *Mycobacterium tuberculosis*, Biochemistry 48 (2009) 1996–2004.

[10] P.A. Frantom, H.M. Zhang, M.R. Emmett, A.G. Marshall, J.S. Blanchard, Mapping of the allosteric network in the regulation of α-isopropylmalate synthase from *Mycobacterium tuberculosis* by the feedback inhibitor L-leucine: solution-phase

H/D exchange monitored by FT-ICR mass spectrometry, Biochemistry 48 (2009) 7457–7464.
[11] F.H. Huisman, N. Koon, E.M. Bulloch, H.M. Baker, E.N. Baker, C.J. Squire, E.J. Parker, Removal of the C-terminal regulatory domain of α-isopropylmalate synthase disrupts functional substrate binding, Biochemistry 51 (2012) 2289–2297.
[12] A.K. Casey, J. Baugh, P.A. Frantom, The slow-onset nature of allosteric inhibition in α-isopropylmalate synthase from *Mycobacterium tuberculosis* is mediated by a flexible loop, Biochemistry 51 (2012) 4773–4775.
[13] N. Koon, C.J. Squire, E.N. Baker, Crystallization and preliminary X-ray analysis of α-isopropylmalate synthase from *Mycobacterium tuberculosis*, Acta Crystallogr. Sect. D: Biol. Crystallogr. 60 (2004) 1167–1169.
[14] C. Follo, C. Isidoro, A fast and simple method for simultaneous mixed site-specific mutagenesis of a wide coding sequence, Biotechnol. Appl. Biochem. 49 (2008) 175–183.
[15] R.J. Leatherbarrow, Grafit Version 6, Erithacus Software Ltd, Horly, United Kingdom, 2007.
[16] P.V. Konarev, V.V. Volkov, A.V. Sokolova, M.H.J. Koch, D.I. Svergun, PRIMUS: a Windows PC-based system for small-angle scattering data analysis, J. Appl. Crystallogr. 36 (2003) 1277–1282.
[17] M.V. Petoukhov, P.V. Konarev, A.G. Kikhney, D.I. Svergun, ATSAS 2.1—towards automated and web-supported small-angle scattering data analysis, J. Appl. Crystallogr. 40 (2007) s223–s228.
[18] D.I. Svergun, Determination of the regularization parameter in indirect-transform methods using perceptual criteria, J. Appl. Crystallogr. 25 (1992) 495–503.
[19] D. Svergun, C. Barberato, M.H. Koch, CRYSOL—a program to evaluate X-ray solution scattering of biological macromolecules from atomic coordinates, J. Appl. Crystallogr. 28 (1995) 768–773.
[20] L. Schrödinger, The PyMOL Molecular Graphics System, Version 1.3r1, 2010.